Solid and Hollow Poly(*p*-xylylene) Particles Synthesis *via* Metal–Organic Framework-Templated Chemical Vapor Polymerization

Salma Begum, Farid Behboodi-Sadabad, Yohanes Pramudya, Christian Dolle, Mariana Kozlowska, Zahid Hassan, Cornelia Mattern, Saleh Gorji, Stefan Heißler, Alexander Welle, Meike Koenig, Wolfgang Wenzel, Yolita M. Eggeler, Stefan Bräse, Joerg Lahann, and Manuel Tsotsalas*

ABSTRACT: Poly(*para*-xylylene)s are a unique class of chemical vapor deposition (CVD)-based polymers, generally referred to their tradename " parylenes", widely used as a protective coating and insulating layer in electronics, especially in printed circuit boards and optical and biomedical devices. Due to their unique synthesis *via* CVD polymerization, parylene coating conforms to a surface; however, molecularly controlled structuring of parylene particles with precise spatial arrangements over multiple hierarchical levels, tailored shapes, sizes, and porosities has not been realized. Here, we report metal–organic framework (MOF)-templated cyclophane-based CVD polymerization with morphology and porosity transcription of the host framework. This catalyst- and initiator-free template approach forms a CVD polymer in three-dimensional (3D) confined nanospaces. The *para*-xylene diradicals (monomers) formed during CVD polymerization using [2.2]paracyclophane (PCP) as a precursor molecule (Gorham process) diffuse into confined nanochannels of the crystalline 3D HKUST-1 MOF and spontaneously polymerize to generate parylene@MOF composites. Here, MOF confined geometries can act as a sacrificial template and, upon removal of the coordinating metal ions, facilitate the formation of templated parylene particles with the transcription of the parent crystal HKUST-1 morphology and porosity. The templated morphologies depend on subtle changes of the chemical composition of the CVD precursors as indicated by clear morphological differences observed for parylene particles synthesized from pristine and chloro-substituted PCPs. Atomistic *ab initio* and classical molecular dynamics simulations and energy barrier calculations using the density functional theory–nudged elastic band method of the poly(*para*-xylylene) precursors in an HKUST-1 confinement were performed to study the mechanism of the molecularly controlled structuring of parylenes. The structuring process is driven by the differences in the diffusion properties of diradicals precursors inside the HKUST-1 MOF. MOF-templated CVD polymerization with implementation of 3D spatial arrangements establishes a new platform for the synthesis of functional parylene polymer particles with structurally controlled morphologies, where molecularly imprinted structuring is modulated by the choice of both the template and the CVD precursor.

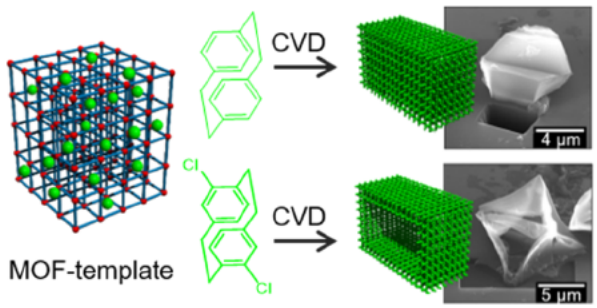

INTRODUCTION

Poly(*para*-xylylene)s (PPXs), generally referred to their tradename as parylenes, a unique class of polymers, are obtained by cyclophane-based chemical vapor deposition (CVD) polymerization for diverse material applications.[1−3] CVD is a versatile process compatible with a range of polymerization modes for making freestanding thin films or coatings on almost any surface and confined microgeometries. The CVD process does not require any catalyst, initiator or solvent. The reactive species from chemical precursors are preformed in the vapor phase and spontaneously polymerize without any side products or decomposition of the monomers.[4] The chemical inertness, high purity, flexibility, mechanical strength, and stability of parylenes offer enormous potential in surface modification, optoelectronics, and drug delivery systems and have demonstrated technological utility for coatings of industrial products (e.g., clinically used biomaterials and biomedical devices).[5−9] Integrating the CVD polymerization process with a template-driven approach can significantly advance capabilities for molecularly controlled structuring of parylenes with tailored shapes, sizes, and

Scheme 1. Schematic Illustration of the Polymerization of Poly(*p*-xylylene) *via* cyclophane-basedCVD Polymerization using MOF Crystals as a Template[a]

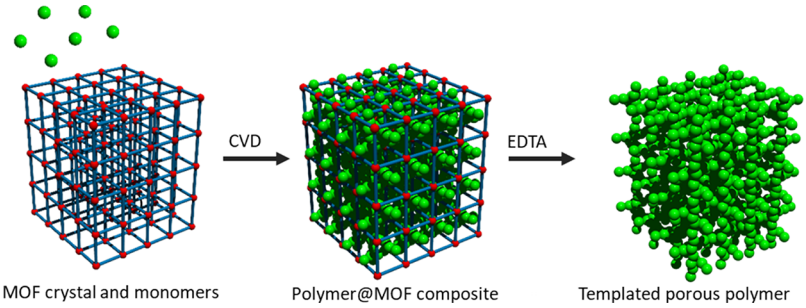

[a]EDTA stands for ethylenediaminetetraacetic acid.

chemistries. Recently, we have used anisotropic liquid crystals as templates to prepare surface-anchored helical nanofibers with programmable shapes and long-range lateral organization.[10] Most notably, by using nematic liquid crystals, straight or bent nanofiber arrays were obtained. By using cholesteric liquid crystals, the helical chirality could be transferred to the nanofibers to template spiraling fibers with tens of μm length. Using chiral PCP precursors bearing a stereogenic center enables the formation of chirality-defined superhierarchical arrays of nanohelices via CVD polymerization into supported films of LCs.[11] This finding outlines a new approach for polymer nanostructures, as morphological design features can be templated aiming for engineered 3D soft-matter architectures. Cyclophane-based CVD polymerization on sublimating ice particles at the dynamic vapor−solid interface has also been introduced to prepare poly(*p*-xylylene) structures, replicating the ice particle template.[12−14] This vapor-phase sublimation and deposition process occurs simultaneously, where the deposition of the poly(*p*-xylylene)s occupies the space vacated by the sublimating ice.

MOFs are synthetic 3D porous crystalline hybrid materials composed of metal-containing nodes and organic ligands that exhibit regular extended structures and have confined pores and channels which can be tailored to serve as molecular-level flasks and scaffolds for controlled polymerization.[15−17] Owing to fascinating structural attributes, MOFs have been demonstrated to be an excellent host,[18] extensively investigated in gas adsorption/separation,[19] molecular recognition,[20] and other emerging applications.[21] For the realization of controlled polymerization using MOF pores and channels, several covalent and noncovalent approaches have been devised to generate MOF−polymer composites with widespread application possibilities.[22−25] Employing MOF nanochannels for the free-radical polymerization of styrene monomers, thereby controlling the macromolecular growth process through the highly ordered geometry of the MOF nanospaces, was pioneered by Kitagawa and co-workers using $[M_2(bdc)_2(dabco)]_n$ (M = Zn^{2+} or Cu^{2+}) (bdc = benzenedicarboxylate; dabco = 1,4-diazabicyclo[2.2.2]octane) together with the initiator 2,2′-azobis(isobutyronitrile).[26] Other relevant studies include oxidative polymerization of pyrrole inside the pores of HKUST-1 ($[Cu_3(BTC)_2]_n$, where BTC = benzene-1,3,5-tricarboxylate)[27] and electrochemical synthesis of polyaniline by employing an HKUST-1-modified conducting electrode,[28] and for introducing chirality with porosity, self-polymerizable chiral monomers (3,4-dihydroxy-L-phenylalanine) have also been immobalized into the pores of an achiral MOF template, resulting in homochiral polymer films that exhibits enantioselective adsorption of naproxen.[29] Similarly, a number of other protocols have been developed to fabricate MOF−polymer hybrid materials with controlled morphologies, including postsynthetic polymerization, grafting, templating, and other bottom-up approaches.[30−35] Pioneering studies on postsynthetic transformation of clickable MOFs (azide-functionalized MOFs) to a polymer gel by Sada and co-workers, who employed alkyne−azide click chemistries in a step-by-step fashion to fabricate MOF-templated porous network polymers, had sparked huge interest for the exploration of MOF-templated polymer networks.[36−38] Advancing the concept of crystal-controlled polymerization in confined nanospaces, we have demonstrated the utility of an epitaxially grown surface-anchored MOF (SURMOF) for structuring polymer networks, forming three-dimensional cross-linked network polymers and interwoven molecular architectures with widespread application possibilities and tunable properties.[39,40] Self-polymerization of the homopolymerizable ligands in the MOF nanospaces to form interwoven polymeric molecular architectures (without the need for guest molecules) has also been demonstrated.[41] Despite the rapid progress of this appealing concept, the key limitations associated to diffusion limitation and blocking of pores with the proceeding reaction, limited stability of MOFs in reaction medium, as well as the requirement of a specific catalyst or initiator and solvent, and long reaction time offer the opportunity for improvements. Moreover, judicious selection and particular design of polymerizable modular building blocks are a prerequisite for enabling such polymerization.[42,43] To overcome some of these hurdles, by combining the cyclophane-based CVD polymerization with a MOF-templated approach, in this report, we sought to develop a new and effective method for structuring of the porous parylene particles *via* crystal-controlled CVD polymerization employing solid-state 3D MOF confined geometries as sacrificial templates (Scheme 1). This is the first report on the cyclophane-based MOF-templated polymerization using the CVD approach, though in the context of MOF−inorganic composites, CVD has been employed in the synthesis of inorganic materials such as metal nanoparticles and organometallic complexes inside the MOF nanochannels.[44,45]

Compared to conventional approaches reported for polymerization in MOFs, the CVD polymerization process offers advantages of (i) clean conversion of the monomers without any byproducts, (ii) does not require initiator- and (iii) solvent-free in nature, and additionally (iv) an efficient

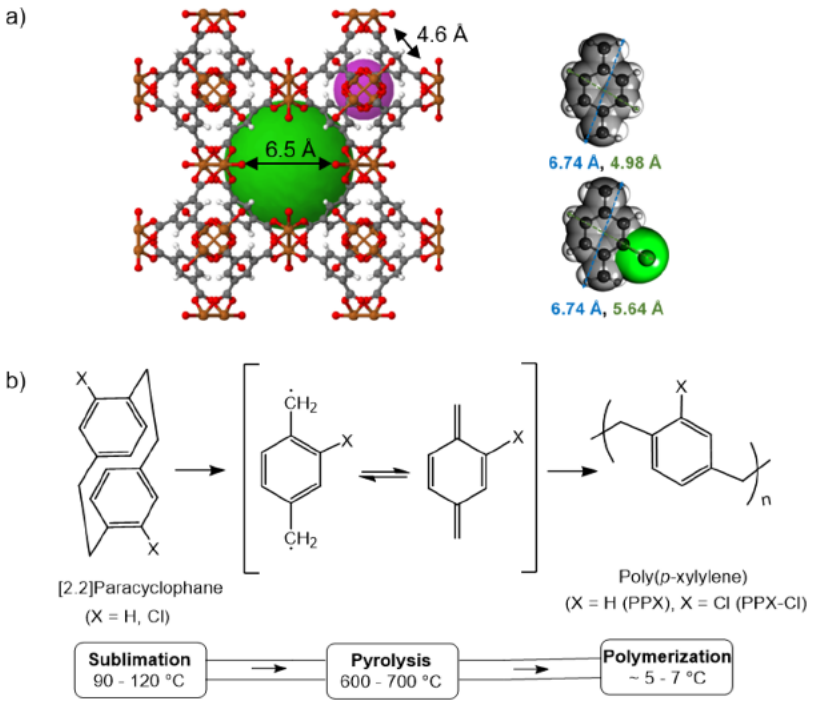

Figure 1. (a) Atomistic representation of the HKUST-1 MOF, where the green and purple spheres represent the pore sizes with pore apertures of 6.5 and 4.6 Å, respectively (source, ChemTube3D), and the dimensions of the PPX and PPX-Cl monomers (radicals) formed during the pyrolysis step of the CVD polymerization; (b) CVD polymerization reactions used in this report to fabricate nanostructured PPX and PPX-Cl polymer particles from different PCPs.

diffusion of the precursors enables homogeneous access of complex geometries, even under nanoscopic confinement.

EXPERIMENTAL SECTION

Materials. All chemicals were purchased from commercial sources and were used without any further purification. $Cu(NO_3)_2{\cdot}3H_2O$, trimesic acid (H_3btc), ethylenediaminetetraacetic acid (EDTA), and rhodamine B were purchased from Sigma Aldrich (Germany). [2.2]Paracyclophane (Curtiss-Wright Surface Technologies, Galway, Ireland) and dichloro-[2.2]paracyclophane (ABCR GmbH, Karlsruhe, Germany) were used as received. HPLC-grade solvents ethanol (absolute, >99.9%) and toluene (>99.8%) were purchased from VWR (Germany).

Synthesis of HKUST-1 MOFs. HKUST-1 was prepared according to the literature procedure.[46] For HKUST-1, $Cu(NO_3)_2{\cdot}3H_2O$ (109 mg, 0.45 mmol) and trimesic acid (H_3btc, 52.5 mg, 0.25 mmol) in a 10 mL solvent mixture of H_2O and ethanol (50% v/v) in a Teflon-lined autoclave were heated at 120 °C for 12 h. After cooling down to 30 °C, the obtained products (blue crystals) were washed with ethanol three times, collected by centrifugation (4000 rpm, 5 min), and stored in ethanol.

Synthesis of Parylene@MOF Composites *via* CVD Polymerization. The parylene@MOF composites were prepared by the chemical vapor deposition (CVD) polymerization method using a custom-built setup. The monomer (40 mg) (PCP (Curtiss-Wright Surface Technologies, Galway, Ireland) or dichloro-PCP (ABCR GmbH, Karlsruhe, Germany) was fed into the CVD setup, and the MOF particles dispersed on a silicon wafer were placed on top of the cooled sample holder in the deposition chamber (see the CVD setup in Scheme S1). In this process, the PCP monomer sublimed at elevated temperatures (90−120 °C) and under a reduced pressure (0.12 mbar). Later, it formed free radicals during the pyrolysis step at 660 °C while flowing through a 320 mm-long quartz tube with the carrier gas (Ar, flow rate of 20 sccm). Finally, polymerization occurred in the deposition chamber where MOF particles dispersed on a silicon wafer were placed on the rotating (30 rpm) substrate, which was equipped with a cooled (~5−7 °C) sample holder.

Preparation of Templated Parylene (PPXs and PPX-Cl) Particles. Parylene (PPXs and PPX-Cl) particles were extracted from the parylene@MOF composites by dissolution of the MOF templates. Parylene@MOF composites were placed in 30% w/v EDTA solution (H_2O/EtOH 50% v/v) at pH 12 (maintained by NaOH solution) for 10 days. HKUST-1 decomposition was monitored by the appearance of a blue color with the gradual release of the copper metal ions. The resultant colorless parylene particles were washed three times with the ethanol−water mixture (50% v/v) and stored in ethanol.

Rhodamine Dye Loading in the Parylene Polymer Particles. PPXs and PPX-CL particles were suspended in 2 mL of rhodamine solution (40 μg/mL in water) at 25 °C for 20 h. The particles settled at the bottom of the vial, the solution was decanted, and particles were washed three times with water. The washed particles were drop-casted on a glass coverslip for digital microscope studies.

Computational Studies. All calculations were performed using the structure of HKUST-1 (reported by Chui et al.)[46] using a fully periodic approach. The quantum simulations were performed using VASP6.2.0.[47]

We used the linearized augmented-plane-wave (LAPW) method to describe the electron wave functions with a default energy cutoff of 400 eV. PBE5.4 pseudopotentials for each of the atoms were used. Gamma point structure minimization was performed with a tolerance for the force on each atom of 0.01 eV/Å or less and a delta energy of 10^{-6} eV using the conjugate gradient method.

For the NEB, we used eight image systems between the initial and final position of the molecules passing the pore. For all systems, force-based relaxations in the NEB calculation, specifically damped molecular dynamics by applying a damping factor of 1, a spring constant of −5, and a time step of 0.1 fs, were used. The energy tolerance was set at 10^{-6} eV, and the maximum force allowed on each individual atom was 0.05 eV/Å.

Ab initio MD simulation was performed in the unit cell of HKUST-1 using a 0.5 fs time step. The Boltzmann random initial velocity distribution was used in both *ab initio* MD at T = 500 K and classical MD at T = 400 K. The classical MD simulations of the MOF were performed in a 3 × 3 × 3 HKUST-1 supercell using the UFF4MOF force field,[48] as implemented in LAMMPS. The UFF4MOF force field

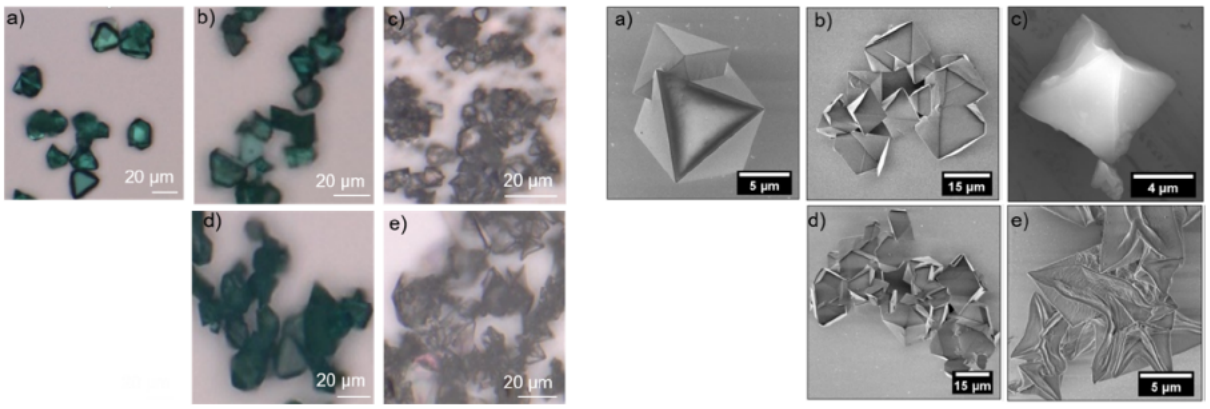

Figure 2. DM (images on the left panel: (a)−(e)) and SEM (images on the right panel: (a)−(e)). For both DM and SEM panels, (a) pristine HKUST-1, (b) PPX@HKUST-1, (c) PPX, (d) PPX-Cl@HKUST-1, and (e) PPX-Cl.

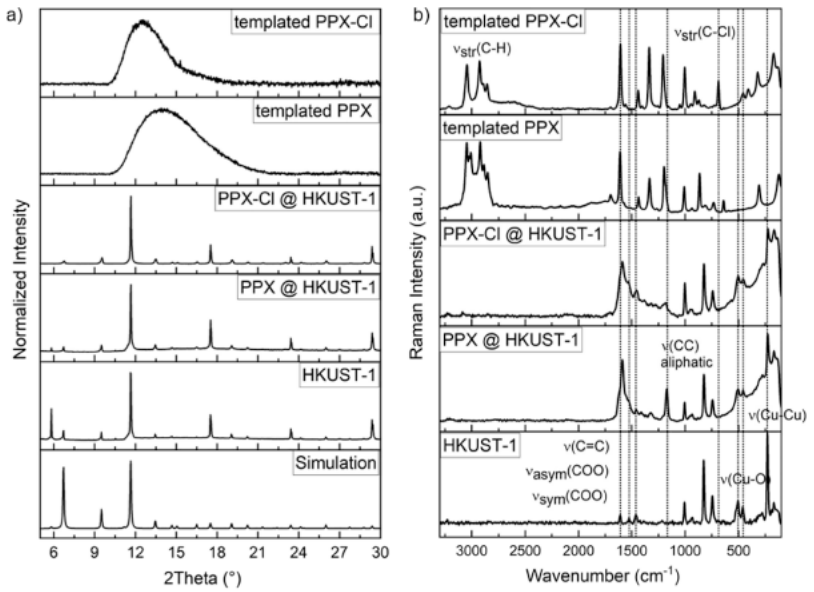

Figure 3. (a) PXRD patterns and (b) Raman spectra collected with λ 532 nm (right) of the pristine HKUST-1, parylene@MOF composites (PPX@HKUST-1 and PPX-Cl@HKUST-1), and parylene particles (PPX and PPX-Cl).

was tested and designed to keep the Cu-paddle wheel secondary building unit in correct topology while still allowing some degree of flexibility of the Cu-paddle wheel. Details of the calculation parameters are provided in the SI.

RESULTS AND DISCUSSION

We commenced our studies using the HKUST-1 MOF as a template for the formation of parylenes in confined nanospaces as a proof of concept. HKUST-1 is a porous open framework constituted by benzene-1,3,5-tricarboxylate organic linkers and Cu-paddle wheel nodes. It contains an intersecting three-dimensional system of large square-shaped pores (9 Å by 9 Å) composed of three types of cages and is largely explored for the adsorption and separation of xylene isomers inside the pores of the HKUST-1 MOF.[46] The smallest cages with an aperture of 4.6 Å (purple sphere in Figure 1a) are not accessible to any xylene isomers, and the two large cages with the internal diameters of 10 and 12 Å with a pore aperture of 6.5 Å (green sphere in Figure 1a) permit selective diffusion/adsorption of xylene isomers.[49]

Comparing the molecular size and structure, *para*-xylene is considered a structural analogue of the CVD monomers where the *para*-xylene dimer [2.2]paracyclophane (PCP)[50−52] is used as a precursor for the PPX formation. Two different PCP precursor molecules (as CVD monomers) of di-*p*-xylylene (nonfunctionalized PCP) and dichlorodi-*p*-xylylene (dichloro-substituted PCP) were chosen to synthesize polymers *via* CVD polymerization in three-dimensional pores within HKUST-1 referred here as PPX and PPX-Cl, respectively (Figure 1). The PCP molecules are cracked homolytically at the ethylene bridges in a custom-built CVD device setup in a standard Gorham process (thereby generating two 1,4-quinodimethane radicals (p-xylylene) in the gas phase, see Figure 1b and Scheme S1). Under the gas flux, these monomers diffuse inside the nanochannels of the 3D HKUST-1 MOF and spontaneously polymerize to generate parylene@MOF composites. The resulting parylene@HKUST-1 composites are named after the corresponding polymers as PPX@HKUST-1 and PPX-Cl@HKUST-1. The HKUST-1 sacrificial template from the parylene@HKUST-1 composite was dissolved by the treatment of EDTA solution. Contrary to the trivial solvent-resistant nature of parylene coatings, we observed the slow diffusion of EDTA solution through the parylene@HKUST-1 composite, resulting in the leaching of copper ions turning the

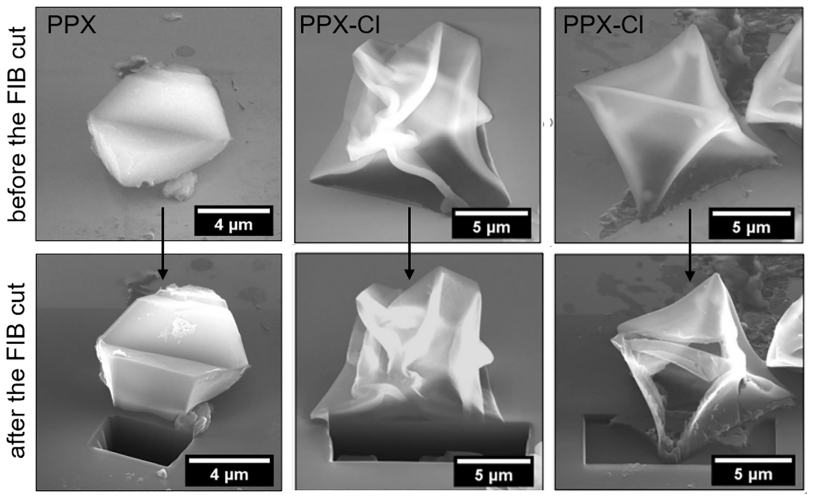

Figure 4. Crystal shape and cross section of the parylene particles PPX and PPX-Cl before and after the FIB cuts.

EDTA colorless solution into blue. Complete removal of the MOF template from the parylene@HKUST-1 composite resulted in colorless parylene particles (PPX and PPX-Cl). Dissolution of the HKUST-1 sacrificial template (hydrolysis and subsequent demetalation) yielded metal-free, entirely organic, templated PPX and PPX-Cl particles as shown in Figure 2.

The pristine HKUST-1, parylene@HKUST-1 composite, and the parylene particle (PPXs and PPX-Cl) samples were studied by a digital microscope (DM) and a scanning electron microscope (SEM) as shown in Figure 2. The DM and SEM images reveal that the pristine morphology of the HKUST-1 is well-preserved by the parylene@HKUST-1 composites and the parylene particles, indicating the successful transfer of nanostructures and structural regularity into the newly formed parylene particles. Taken together, the data obtained by DM and SEM studies suggest that CVD polymerization successfully deposited the polymers in the confined nanochannels of HKUST-1. The samples were further characterized by powder X-ray diffraction (PXRD), attenuated total reflectance (ATR), Raman spectroscopy, time-of-flight secondary-ion mass spectrometry (ToF-SIMS), SEM with energy-dispersive X-ray elemental mapping (SEM−EDX), and focused ion beam scanning electron microscopy (FIB-SEM).

Crystallinity of the parent HKUST-1, parylene@HKUST-1 composites, and the parylene particles (PPX and PPX-Cl) was evaluated by PXRD analysis. As shown in Figure 3a, PXRD data of the pristine MOF HKUST-1 and parylene@HKUST-1 composites overall match well with the HKUST-1 reference pattern. XRD patterns of the HKUST-1 before and after the CVD polymerization showed identical peak positions, indicating that the parent MOF network structure is kept intact during the CVD polymerization. The MOF-templated CVD approach afforded semicrystalline parylene particles, each exhibiting a broad peak. PPX and PPX-Cl peak positions and respective shifts are in agreement with the literature.[53] The different peak positions are due to the variation in the distribution of crystalline domains of PPX and PPX-Cl. From the PXRD pattern, domain sizes of around 13 and 30 Å can be calculated for PPX and PPX-Cl, respectively. Based on the molecular sizes of PPX (6.3 Å) and PPX-Cl (7 Å), roughly two and five molecules in each direction, respectively, are arranged in small aggregates in the range of the observed few angstroms. Thus, they can form different periodic structures leading to different positions of the very broad peaks as found in the corresponding diffractogram.

MOF−polymer composites are further characterized by thermogravimetric analysis (TGA), and TGA graphs are provided in the SI (Figure S2). TGA graphs show the first weight loss of solvent molecules in the temperature range of 40−245 °C. The plateau of dehydrated/desolvated samples is adjusted to 100%. The HKUST-1 structure is decomposed around 310 °C with a weight loss of 35% ascribed to the loss of organic linker molecules. In comparison to this, weight losses of around 43 and 45% in the case of composites PPX@HKUST-1 and PPX-Cl@HKUST-1 infer that the composites contain around 8 and 10% more organic content than the pristine HKUST-1, respectively. We further verified the PPX and PPX-Cl polymer formation by Raman and ATR-IR spectroscopy. The Raman spectra (Figure 3b and Figure S1) are consistent and fit well with the literature.[54,55] The bands associated with the Cu ions in HKUST-1 appear between 150 and 600 cm^{-1}. The bands at 505 and 457 cm^{-1} and in the range of 193−172 cm^{-1} and a band at 230 cm^{-1} are attributed to Cu−O (oxygen atoms of carboxylate bridges) and Cu−Cu stretching modes, respectively. The Raman modes at 1467 and 1388 cm^{-1} are assigned to the asymmetric and symmetric stretching vibrations of carboxylate (COO) groups. Comparing the HKUST-1 Raman spectrum with the Raman spectra of PPX@HKUST-1 and PPX-Cl@HKUST-1, the characteristic bands associated with Cu ions and carboxylate groups appeared at the same positions with no spectral shifts. This observation suggests that the polymers are not interacting with the copper metal node and the template structure remains intact. In the composite sample of parylene@HKUST-1, the bands at 1175, 1322, and 1588 cm^{-1} are associated with the PPX and PPX-Cl polymers. Raman bands around 1200 cm^{-1} originate from aliphatic (C−C) chain vibrations. The parylene particles (PPX and PPX-Cl) exhibit strong Raman bands (2800−3200 cm^{-1}) that correspond to the vibrational stretches of the C−H bond. The medium region at 1450 cm^{-1} is assigned to the C−C bond and the lowermost region at 800 cm^{-1} to the deformation vibration of the C−C bond. At 1609 cm^{-1}, the C═C symmetric stretching of the benzene ring is recognized; in the case of composites, this band is slightly shifted and appeared at 1589 cm^{-1}, which can be

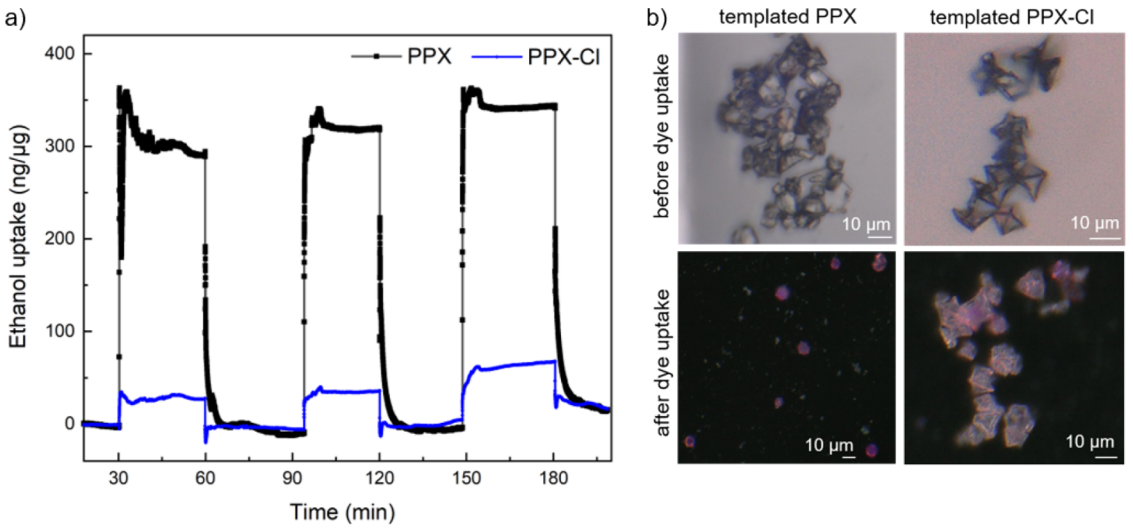

Figure 5. Vapor sorption and dye uptake study of templated PPX and PPX-Cl polymers. (a) Ethanol vapor uptake (QCM data) in templated polymers PPX (black) and PPX-Cl (blue). The ethanol vapor uptake is presented as a function of time in three repeated cycles. (b) Digital microscope images before and after the rhodamine dye uptake in parylene particles PPX and PPX-Cl.

ascribed to the template effect.[56] A similar trend of shifts in frequency is observed for the PPX (1195 and 1334 cm^{-1}) and PPX-Cl bands (1208 and 1334 cm^{-1}) in reference to the corresponding spectra of PPX@HKUST-1 and PPX-Cl@HKUST-1. In the parylene particles (PPX and PPX-Cl), the bands associated with HKUST-1 completely disappeared, confirming successful removal of the MOF template from the composites after dissolution of the HKUST-1. ATR-IR spectra agree with the Raman studies (Figure S2).

Furthermore, SEM−EDX and ToF-SIMS elemental mapping (Figures S3 and S7) show the absence of copper and oxygen atoms as expected due to the removal of HKUST-1 from the PPX and PPX-Cl particles. On careful look on the depth-integrated ToF-SIMS image (Figure S6), traces of copper ions in some particles of PPX-Cl are observed. For complete removal of copper ions, polymer@HKUST-1 composites were placed in the basic EDTA (pH 12) solution for two weeks. In comparison to the PPX polymer, PPX-Cl polymer particles need a longer time for removal of copper ions. A tropylium cation ($C_7H_7^+$) fragment is observed in the case of the PPX@HKUST-1 composite, indicating the presence of the parylene polymer: ionization causes the formation of benzyl fragments, which rearrange to the highly stable tropylium cation. The presence of $^{65}CuCl_2^-$ and $CuCl_2^-$ (Figure S5) in the depth-integrated images of the composite PPX-Cl@HKUST-1 exhibits the correlation of copper (from HKUST-1) and chlorine (from PPX-Cl) distribution. This confirms the diffusion of PPX-Cl monomers inside the HKUST-1 and formation of the MOF polymer composite (PPX-Cl@HKUST-1) to the extent of around 100 nm in the range of ToF-SIMS accessible depths.

To confirm the micrometer-scale penetration depth of the parylene polymers within the MOF template and to verify its modulation by the choice of monomer precursors, such as in the case of PPX and PPX-Cl, FIB-SEM studies were performed. The focused ion beam mills the sample surface *via* a sputtering process. The stepwise gradual milling allows us to get insight into the inner packing of particles, revealing whether the particles are filled or hollow inside. Figure 4 shows PPX and PPX-Cl parylene polymer particles before and after the FIB cuts: the PPX cross section displays a solid core, whereas in the case of PPX-Cl, hollow particles are observed. This shows direct evidence that polymerization in the case of PPX@MOF happens inside the HKUST-1 nanochannels over the whole MOF, whereas for PPX-Cl@MOF, it proceeds mostly on the exterior and polymerization inside the MOF nanochannels is hindered.

Hampered polymerization inside the MOF nanochannels therefore attained hollow structures, a consequence of the squeezed octahedron morphology of the PPX-Cl particles. Computational analysis (*vide infra*) of both PPX and PPX-Cl polymer systems revealed differences in the diffusion of the corresponding CVD monomers (depicted in Figure 1a) within the MOF pores and consequently the probability of radical polymerization inside the MOF pores. FIB-SEM observations, together with the calculated diffusion energy barriers of the monomers in HKUST-1, confirm different types of parylene particles obtained in the CVD, even if the precursor PCP molecules differ only with one atom substitution, i.e., Cl instead of H. This reveals the high selectivity of the MOF template and opens a new pathway toward predictive design of new nanotemplated parylene particles.

In accordance with our findings on the precursor-modulated solid and hollow parylene particles, significant differences in the transcription of porosity *via* an MOF-templated approach in the PPX and PPX-Cl polymers are plausible as well. To evaluate the sorption behavior of both materials with anticipated void spaces, we studied ethanol sorption by quartz crystal microgravimetry using a quartz crystal microbalance (QCM) (Figure 5a) and by rhodamine dye uptake (Figure 5b). The QCM measures the change in frequency (Δf); based on the Sauerbrey equation, Δf is directly related to the change in mass that gives insight into the loading capacity and is a useful tool for organic vapor sorption with high sensitivity.[57] For sorption of ethanol in the vapor state, a parylene particle (PPX and PPX-Cl) suspension in ethanol was drop-casted on the QCM gold sensor. Samples were dried and *in situ* activated at 50 °C under N_2 flow for 24 h. PPX and PPX-Cl drop-casted samples and the reference (bare gold QCM sensor) were assembled into three channels of the QCM device and measured in parallel to assure real-time monitoring with the additional advantage of consistency for comparative studies.

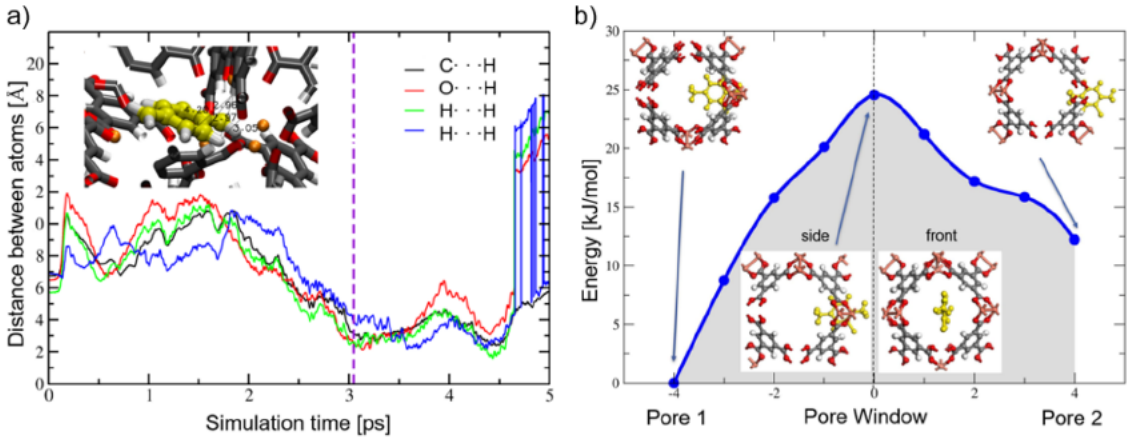

Figure 6. (a) The *y*-axis is the intermolecular distance between the PPX precursor and the MOF scaffold during crossing the pore aperture. The dashed line represents the time when the diffusion of the molecule from one pore to the other occurs, and the distance between PPX and the nearest HKUST-1 atom is at the minimum. (b) Nudged elastic band (NEB) diffusion energy barrier of the monomer of the PPX-Cl (yellow) inside the HKUST-1 MOF. The *x*-axis represents the position of the molecules relative to the pore aperture ($x = 0$). The *y*-axis is the energy of the system and shows a diffusion energy barrier of 25 kJ/mol.

For the assembled samples, Δf was recorded (Figure S9) under N_2 flow (referenced baseline), with loading of 100% saturation vapor pressure of ethanol (N_2 flow was saturated with the ethanol vapors at 25 °C). A pronounced increase in mass uptake (~320 ng/μg) is observed upon exposure of the PPX sample to the ethanol vapors in three repeated cycles, while for the PPX-Cl, comparatively less mass uptake (~40 ng/μg) is recorded. Sensorgrams of ethanol in three repeated cycles for PPX and PPX-Cl show excellent reversibility of the absorption/desorption processes. Under similar experimental conditions, the mass uptake is contributed mainly by the ethanol vapor loading, suggesting that the PPX particles are porous and hold capacity for ethanol sorption in comparison to the PPX-Cl particles that behave very similar to the reference sensor (Figure S9). Furthermore, rhodamine dye uptake in the PPX and PPX-Cl polymer particles was studied by digital microscopy (Figure 5b). The PPX particles adsorbed qualitatively more dye and exhibited a dark pink color in comparison to the PPX-Cl with a light pink color. The dye uptake in the PPX and PPX-Cl polymer particles agrees with the QCM studies.

COMPUTATIONAL STUDIES

To understand the atomistic details of the observed differences in the MOF-templated PPX and PPX-Cl particles, quantum and classical mechanics simulations of the corresponding monomers inside the 3D HKUST-1 MOF were performed. We started with the structure minimization of the fully periodic HKUST-1 in a quantum level with density functional theory (DFT). The obtained MOF structure was used to study the diffusion of the PPX and PPX-Cl monomers (see Figure 1) using *ab initio* (quantum) and classical molecular dynamics (MD). The NVT *ab initio* MD was performed for 9.5 ps in VASP at 500 K (for accelerating the dynamics of the system) using vdW-B86b functionals that incorporated van der Waals correction.[58] Starting from the PPX monomers with an HKUST-1 pore aperture of 6.5 Å (green sphere in Figure 1a), we observed that the PPX monomer easily diffuses from one MOF pore to the other within 3 ps. Dynamical behavior of the monomers at MOF nanopores and the process of crossing both pores are depicted in Figures S10 and S12. When passing from one pore to the other, intermolecular distances between the PPX monomer and the atoms of the MOF are relatively small, i.e., in the range of 2−3 Å (see Figure 6a). Facile diffusion of the PPX monomers is possible in the ps timescale; on the contrary, the PPX-Cl monomer was not able to pass the pore aperture within 9.5 ps, hindered by the larger size of the monomer due to the presence of Cl atoms (see Figure 6b and Figure S11) and the relatively narrow pore aperture.

To observe the diffusion of the molecules on larger timescales, classical MD simulation for 295 ns in the NVT ensemble at 400 K was performed. Here, significant differences in the diffusion of both PPX and PPX-Cl monomers were observed. PPX monomers easily diffused inside the MOF nanopores and escaped to the neighboring pores within a 3.7 ns simulation time. Meanwhile, the PPX-Cl monomers crossed the pore aperture within 170 ns. These observations suggest that the energy barrier to pass the pore apertures is still below 40 kJ/mol.[59,60] It means that the diffusion of the PPX-Cl monomer inside MOF nanopores is possible under normal conditions but with a significantly slower diffusion rate in comparison to the PPX monomers that diffuse with practically no measurable energy barrier.

To quantify the energy barrier for the monomer passing the pore aperture, we performed DFT−nudged elastic band (NEB) calculations.[61,62] This method allows us to calculate the energy barrier directly if the location of the local minima on the both sides of the pore aperture is found. The energy barrier for the diffusion of the monomers can be calculated from the saddle point, obtained in the NEB procedure.[63] From several trials of the NEB diffusion paths of the PPX-Cl monomer in HKUST-1, the lowest energy barrier was found to be 25 kJ/mol, shown in Figure 6b. The effect of temperature, molecular vibrations, and zero-point energy is relatively small compared to the energy barrier found by the NEB.[64]

The energy barrier of 25 kJ/mol is indeed significant but still allows the PPX-Cl monomer to diffuse within experimental process time. However, the existence of the energy barrier delays the diffusion rate by a factor of 22,000 compared to the nonchlorinated PPX monomer. Therefore, a macroscopic difference of the polymerized material is expected and observed in the experiments. A slower diffusion rate and a longer time inside the MOF pore, in addition to the initially high concentrations of monomers at the MOF exterior during

deposition, may induce the polymerization reaction even before the PPX-Cl monomer is able to diffuse deep inside the MOF. Most of the polymerization reactions are expected to happen at the first few-layer depth of the HKUST-1 surface on diffusion of the PPX-Cl monomers, whereas diffusion of oligomers will be significantly suppressed. This explains well the experimentally observed hollow PPX-Cl polymer particles. In contrast to PPX-Cl, PPX monomers can easily diffuse inside the MOF nanopores, where polymerization resulting in filled PPX particles with the morphology transcription of the parent MOF template is triggered.

Polymerization of the parylene may be influenced by the type of surface used for the deposition, especially when it consists of transition metals. The exposure of CVD monomers to transition metals, metal salts, and organometallic complexes, such as those of iron, ruthenium, platinum, palladium, copper, and silver, is found to inhibit polymer deposition on the substrate.[65−67] In our studies, no changes in the XRD peak positions and Raman bands (Figure 3) associated with copper ions in HKUST-1 before and after the polymerization confirm no significant interactions of monomers with the copper sites. In the HKUST-1 MOF, copper ions are coordinated with the organic linker *via* carboxylate groups; thus, metal centers are not directly accessible. Furthermore, template porosity and fast diffusion of monomers inside the MOF followed by fast polymerization limit the possibility of monomers to interact with metal sites and impact the polymerization mechanism, e.g., *via* inhibition observed in cases where no additional geometrical constraints were applied to the polymer prepared.[65,66]

CONCLUSIONS

In summary, we have developed a new synthetic strategy for structuring parylene polymeric particles with confined morphologies and porosity transcription without the need for a catalyst or initiator *via* solvent-free cyclophane-based chemical vapor polymerization employing crystalline solid-state 3D HKUST-1 MOF confined geometries as a sacrificial template. As a proof of concept, the three-dimensional porous structure of HKUST-1 was studied as a representative system for the synthesis of templated poly(*p*-xylylene) solid and hollow particles *via* CVD modulated by the design of [2.2]paracyclophane precursors. The most important advantages of the CVD are the gas-phase diffusion of monomers in the MOF nanochannels and the ability to access even complex geometries homogeneously. The PPX cross section displays an inside filled solid core, whereas in the case of PPX-Cl, hollow particles are observed. Differences in the morphology and porosity of the PPX and PPX-Cl polymer particles are mainly related to different dynamical behaviors of precursors and their diffusion in the MOF nanopores. *Ab initio* MD simulations reveal picosecond timescale diffusion of the PPX monomers while nanosecond diffusion of the PPX-Cl monomers in the MOF at 500 K. Furthermore, NEB calculations reveal the barrier-free diffusion of the PPX monomers in the HKUST-1 and a barrier of 25 kJ/mol for the chloro-substituted PPX-Cl monomers. This is caused by the small interatomic distances between the precursor and the MOF pore aperture during crossing the pores and the larger size of the chloro-substituted monomers. Our studies reveal the high selectivity of the HKUST-1 MOF template and opens a new pathway toward predictive design of new nanotemplated parylene particles. MOF-templated CVD polymerization by exploiting the structural diversity of MOF crystalline networks with large pores, crystal sizes, and shapes in CVD polymerization establishes a new platform for synthesizing parylenes with structurally controlled morphologies, where molecularly imprinted structuring is modulated by choice of both the host template and the CVD precursors. The synthetic design of the fundamental cyclophane precursors with chemical functionalities that are compatible with CVD conditions and can be immobilized inside the MOF crystalline networks (such as thiol, hydroxyl, and amino groups)[68−72] would be a crucial step. These chemical functionalities, subsequent to the polymerization, can be used as anchoring sites for tailoring post-CVD surface engineering,[73] tremendously increasing the potential for molecularly controlled parylene-derived porous functional materials.

ASSOCIATED CONTENT

Supporting Information

The Supporting Information is available free of charge at https://pubs.acs.org/doi/10.1021/acs.chemmater.2c00111.

Additional Raman spectra, ATR spectra, ToF-SIMS data, SEM−EDX elemental maps, FIB-SEM cross section, QCM data, and details of computational studies (PDF)

AUTHOR INFORMATION

Corresponding Author

Manuel Tsotsalas − *Institute of Functional Interfaces (IFG), Karlsruhe Institute of Technology (KIT), D-76344 Eggenstein-Leopoldshafen, Germany; Institute of Organic Chemistry, Karlsruhe Institute of Technology (KIT), 76131 Karlsruhe, Germany;* orcid.org/0000-0002-9557-2903; Email: manuel.tsotsalas@kit.edu

Authors

Salma Begum − *Institute of Functional Interfaces (IFG), Karlsruhe Institute of Technology (KIT), D-76344 Eggenstein-Leopoldshafen, Germany; Institute of Organic Chemistry, Karlsruhe Institute of Technology (KIT), 76131 Karlsruhe, Germany;* orcid.org/0000-0001-9919-3073

Farid Behboodi-Sadabad − *Institute of Functional Interfaces (IFG), Karlsruhe Institute of Technology (KIT), D-76344 Eggenstein-Leopoldshafen, Germany*

Yohanes Pramudya − *Institute of Nanotechnology (INT), Karlsruhe Institute of Technology (KIT), D-76344 Eggenstein-Leopoldshafen, Germany;* orcid.org/0000-0002-0950-7655

Christian Dolle − *Microscopy of Nanoscale Structures & Mechanisms (MNM), Laboratory for Electron Microscopy (LEM), Karlsruhe Institute of Technology (KIT), Karlsruhe 76131, Germany;* orcid.org/0000-0003-1503-9744

Mariana Kozlowska − *Institute of Nanotechnology (INT), Karlsruhe Institute of Technology (KIT), D-76344 Eggenstein-Leopoldshafen, Germany*

Zahid Hassan − *Institute of Organic Chemistry, Karlsruhe Institute of Technology (KIT), 76131 Karlsruhe, Germany;* orcid.org/0000-0001-5011-9905

Cornelia Mattern − *Institute of Organic Chemistry, Karlsruhe Institute of Technology (KIT), 76131 Karlsruhe, Germany*

Saleh Gorji − *Institute of Nanotechnology (INT), Karlsruhe Institute of Technology (KIT), D-76344 Eggenstein-Leopoldshafen, Germany*

Stefan Heißler − *Institute of Functional Interfaces (IFG), Karlsruhe Institute of Technology (KIT), D-76344 Eggenstein-Leopoldshafen, Germany*
Alexander Welle − *Institute of Functional Interfaces (IFG), Karlsruhe Institute of Technology (KIT), D-76344 Eggenstein-Leopoldshafen, Germany;* orcid.org/0000-0002-3454-6509
Meike Koenig − *Institute of Functional Interfaces (IFG), Karlsruhe Institute of Technology (KIT), D-76344 Eggenstein-Leopoldshafen, Germany;* orcid.org/0000-0003-3150-8723
Wolfgang Wenzel − *Institute of Nanotechnology (INT), Karlsruhe Institute of Technology (KIT), D-76344 Eggenstein-Leopoldshafen, Germany;* orcid.org/0000-0001-9487-4689
Yolita M. Eggeler − *Microscopy of Nanoscale Structures & Mechanisms (MNM), Laboratory for Electron Microscopy (LEM), Karlsruhe Institute of Technology (KIT), Karlsruhe 76131, Germany*
Stefan Bräse − *Institute of Organic Chemistry, Karlsruhe Institute of Technology (KIT), 76131 Karlsruhe, Germany; Institute of Biological and Chemical Systems (IBCS-FMS), Karlsruhe Institute of Technology (KIT), 76344 Eggenstein-Leopoldshafen, Germany*
Joerg Lahann − *Institute of Functional Interfaces (IFG), Karlsruhe Institute of Technology (KIT), D-76344 Eggenstein-Leopoldshafen, Germany; Biointerfaces Institute and Departments of Biomedical Engineering and Chemical Engineering, University of Michigan, Ann Arbor, Michigan 48109, United States;* orcid.org/0000-0002-3334-2053

Author Contributions

The manuscript was written through contributions of all authors. All authors have given approval to the final version of the manuscript.

Notes

The authors declare no competing financial interest.

ACKNOWLEDGMENTS

The German Research Foundation (formally Deutsche Forschungsgemeinschaft (DFG)) in the framework of Cooperative Research Centre "Molecular Structuring of Soft Matter" (Sonderforschungsbereich (SFB) 1176) and the Cluster "3D Matter Made to Order" under Germany's Excellence Strategy (3DMM2O EXC-2082−390761711, Thrust A1 and A2) is greatly acknowledged for financial contributions. Y.P. and W.W. acknowledge support of the DFG WE 1863/29-1 and Hoch Performance flüssig-prozessierte keramische Solarzellen (KeraSolar) funded by the Karlsruhe Institute of Technology (KIT) and Carl-Zeiss-Stiftung. M.K. acknowledges funding by the Ministry of Science, Research and Art of Baden-Württemberg Germany under the Brigitte-Schlieben-Lange Program. S.G. thanks the Deutsche Akademische Austauschdienst (DAAD) for a doctoral scholarship. We thank Dr. Torsten Scherer (INT, KIT) and Prof. Dr. Christian Kübel (INT, KIT) for stimulating discussions and acknowledge support for FIB analysis by the Karlsruhe Nano Micro Facility (KNMF, http://www.knmf.kit.edu/). We thank Birgit Huber (Soft Matter Synthesis Laboratory, IBG3, KIT) for providing support in thermogravimetric analysis. M.T. gratefully acknowledges the Helmholtz Association's Initiative and Networking Fund (grant VH- NG-1147) for financial contributions.

REFERENCES

(1) Deng, X.; Cheng, K. C. K.; Lahann, J., Multifunctional Reactive Polymer Coatings. In *CVD Polymers: Fabrication of Organic Surfaces and Device*, Gleason, K. K., Ed. Wiley-VCH: Weinheim, 2015; pp. 199−216.
(2) Klee, D.; Weiss, N.; Lahann, J., Vapor-Based Polymerization of Functionalized [2.2]Paracyclophanes: A Unique Approach towards Surface-Engineered Microenvironments. In *Modern Cyclophane Chemistry*, Gleiter, R.; Hopf, H., Eds. Wiley-VCH: Weinheim, 2004; pp. 463−484.
(3) Gorham, W. F. A New, General Synthetic Method for the Preparation of Linear Poly-p-xylylenes. *J. Polym. Sci., Part A-1: Polym. Chem.* **1966**, *4*, 3027−3039.
(4) Moss, T.; Greiner, A. Functionalization of Poly(para-xylylene)-s—Opportunities and Challenges as Coating Material. *Adv. Mater. Interfaces* **2020**, *7*, 1901858.
(5) Deng, X.; Lahann, J. Orthogonal surface functionalization through bioactive vapor-based polymer coatings. *J. Appl. Polym. Sci.* **2014**, *131* (), DOI: 10.1002/app.40315.
(6) Chen, H.-Y.; Lahann, J. Designable Biointerfaces Using Vapor-Based Reactive Polymers. *Langmuir* **2011**, *27*, 34−48.
(7) Deng, X.; Friedmann, C.; Lahann, J. Bio-orthogonal "Double-Click" Chemistry Based on Multifunctional Coatings. *Angew. Chem., Int. Ed.* **2011**, *50*, 6522−6526.
(8) Asatekin, A.; Barr, M. C.; Baxamusa, S. H.; Lau, K. K. S.; Tenhaeff, W.; Xu, J.; Gleason, K. K. Designing polymer surfaces via vapor deposition. *Mater. Today* **2010**, *13*, 26−33.
(9) Nandivada, H.; Chen, H.-Y.; Bondarenko, L.; Lahann, J. Reactive Polymer Coatings that "Click". *Angew. Chem., Int. Ed.* **2006**, *45*, 3360−3363.
(10) Cheng, K. C. K.; Bedolla-Pantoja, M. A.; Kim, Y.-K.; Gregory, J. V.; Xie, F.; de France, A.; Hussal, C.; Sun, K.; Abbott, N. L.; Lahann, J. Templated nanofiber synthesis via chemical vapor polymerization into liquid crystalline films. *Science* **2018**, *362*, 804−808.
(11) Varadharajan, D.; Nayani, K.; Zippel, C.; Spuling, E.; Cheng, K. C.; Sarangarajan, S.; Roh, S.; Kim, J.; Trouillet, V.; Bräse, S.; Abbott, N. L.; Lahann, J. Surfaces Decorated with Enantiomorphically Pure Polymer Nanohelices via Hierarchical Chirality Transfer across Multiple Length Scales. *Adv. Mater.* **2022**, *34*, 2108386.
(12) Tung, H.-Y.; Guan, Z.-Y.; Liu, T.-Y.; Chen, H.-Y. Vapor sublimation and deposition to build porous particles and composites. *Nat. Commun.* **2018**, *9*, 2564.
(13) Chiu, Y.-R.; Hsu, Y.-T.; Wu, C.-Y.; Lin, T.-H.; Yang, Y.-Z.; Chen, H.-Y. Fabrication of Asymmetrical and Gradient Hierarchy Structures of Poly-p-xylylenes on Multiscale Regimes Based on a Vapor-Phase Sublimation and Deposition Process. *Chem. Mater.* **2020**, *32*, 1120−1130.
(14) Wu, C.-Y.; Wu, T.-Y.; Guan, Z.-Y.; Wang, P.-Y.; Yang, Y.-C.; Huang, C.-W.; Lin, T.-H.; Chen, H.-Y. Vapor-phased fabrication and modulation of cell-laden scaffolding materials. *Nat. Commun.* **2021**, *12*, 3413.
(15) Zhou, H.-C. J.; Kitagawa, S. Metal−Organic Frameworks (MOFs). *Chem. Soc. Rev.* **2014**, *43*, 5415−5418.
(16) Zhou, H.-C.; Long, J. R.; Yaghi, O. M. Introduction to Metal−Organic Frameworks. *Chem. Rev.* **2012**, *112*, 673−674.
(17) Long, J. R.; Yaghi, O. M. The pervasive chemistry of metal−organic frameworks. *Chem. Soc. Rev.* **2009**, *38*, 1213−1214.
(18) Drake, T.; Ji, P.; Lin, W. Site Isolation in Metal−Organic Frameworks Enables Novel Transition Metal Catalysis. *Acc. Chem. Res.* **2018**, *51*, 2129−2138.
(19) Islamoglu, T.; Chen, Z.; Wasson, M. C.; Buru, C. T.; Kirlikovali, K. O.; Afrin, U.; Mian, M. R.; Farha, O. K. Metal−Organic Frameworks against Toxic Chemicals. *Chem. Rev.* **2020**, *120*, 8130−8160.

(20) Chen, B.; Xiang, S.; Qian, G. Metal−Organic Frameworks with Functional Pores for Recognition of Small Molecules. *Acc. Chem. Res.* **2010**, *43*, 1115−1124.
(21) Dincă, M.; Long, J. R. Introduction: Porous Framework Chemistry. *Chem. Rev.* **2020**, *120*, 8037−8038.
(22) Begum, S.; Hassan, Z.; Brase, S.; Tsotsalas, M. Polymerization in MOF-Confined Nanospaces: Tailored Architectures, Functions, and Applications. *Langmuir* **2020**, *36*, 10657−10673.
(23) Kalaj, M.; Bentz, K. C.; Ayala, S.; Palomba, J. M.; Barcus, K. S.; Katayama, Y.; Cohen, S. M. MOF-Polymer Hybrid Materials: From Simple Composites to Tailored Architectures. *Chem. Rev.* **2020**, *120*, 8267−8302.
(24) Schmidt, B. V. K. J. Metal-Organic Frameworks in Polymer Science: Polymerization Catalysis, Polymerization Environment, and Hybrid Materials. *Macromol. Rapid Commun.* **2020**, *41*, 1900333.
(25) Kitao, T.; Zhang, Y.; Kitagawa, S.; Wang, B.; Uemura, T. Hybridization of MOFs and polymers. *Chem. Soc. Rev.* **2017**, *46*, 3108−3133.
(26) Uemura, T.; Kitagawa, K.; Horike, S.; Kawamura, T.; Kitagawa, S.; Mizuno, M.; Endo, K. Radical polymerisation of styrene in porous coordination polymers. *Chem. Commun.* **2005**, *48*, 5968−5970.
(27) Uemura, T.; Kadowaki, Y.; Yanai, N.; Kitagawa, S. Template Synthesis of Porous Polypyrrole in 3D Coordination Nanochannels. *Chem. Mater.* **2009**, *21*, 4096−4098.
(28) Lu, C.; Ben, T.; Xu, S.; Qiu, S. Electrochemical Synthesis of a Microporous Conductive Polymer Based on a Metal−Organic Framework Thin Film. *Angew. Chem., Int. Ed.* **2014**, *53*, 6454−6458.
(29) Gu, Z.-G.; Fu, W.-Q.; Liu, M.; Zhang, J. Surface-mounted MOF templated fabrication of homochiral polymer thin film for enantioselective adsorption of drugs. *Chem. Commun.* **2017**, *53*, 1470−1473.
(30) Uemura, T.; Yanai, N.; Kitagawa, S. Polymerization reactions in porous coordination polymers. *Chem. Soc. Rev.* **2009**, *38*, 1228−1236.
(31) Zimpel, A.; Preiß, T.; Röder, R.; Engelke, H.; Ingrisch, M.; Peller, M.; Rädler, J. O.; Wagner, E.; Bein, T.; Lächelt, U.; Wuttke, S. Imparting Functionality to MOF Nanoparticles by External Surface Selective Covalent Attachment of Polymers. *Chem. Mater.* **2016**, *28*, 3318−3326.
(32) Mochizuki, S.; Kitao, T.; Uemura, T. Controlled polymerizations using metal−organic frameworks. *Chem. Commun.* **2018**, *54*, 11843−11856.
(33) Oaki, Y.; Sato, K. Crystal-controlled polymerization: recent advances in morphology design and control of organic polymer materials. *J. Mater. Chem. A* **2018**, *6*, 23197−23219.
(34) Zimpel, A.; Al Danaf, N.; Steinborn, B.; Kuhn, J.; Höhn, M.; Bauer, T.; Hirschle, P.; Schrimpf, W.; Engelke, H.; Wagner, E.; Barz, M.; Lamb, D. C.; Lächelt, U.; Wuttke, S. Coordinative Binding of Polymers to Metal−Organic Framework Nanoparticles for Control of Interactions at the Biointerface. *ACS Nano* **2019**, *13*, 3884−3895.
(35) Legrand, A.; Liu, L.-H.; Royla, P.; Aoyama, T.; Craig, G. A.; Carné-Sánchez, A.; Urayama, K.; Weigand, J. J.; Lin, C.-H.; Furukawa, S. Spatiotemporal Control of Supramolecular Polymerization and Gelation of Metal−Organic Polyhedra. *J. Am. Chem. Soc.* **2021**, *143*, 3562−3570.
(36) Anan, S.; Mochizuki, Y.; Kokado, K.; Sada, K. Step-Growth Copolymerization Between an Immobilized Monomer and a Mobile Monomer in Metal−Organic Frameworks. *Angew. Chem., Int. Ed.* **2019**, *58*, 8018−8023.
(37) Ishiwata, T.; Kokado, K.; Sada, K. Anisotropically Swelling Gels Attained through Axis-Dependent Crosslinking of MOF Crystals. *Angew. Chem., Int. Ed.* **2017**, *56*, 2608−2612.
(38) Ishiwata, T.; Furukawa, Y.; Sugikawa, K.; Kokado, K.; Sada, K. Transformation of Metal−Organic Framework to Polymer Gel by Cross-Linking the Organic Ligands Preorganized in Metal−Organic Framework. *J. Am. Chem. Soc.* **2013**, *135*, 5427−5432.
(39) Begum, S.; Hassan, Z.; Bräse, S.; Wöll, C.; Tsotsalas, M. Metal-Organic Framework-Templated Biomaterials: Recent Progress in Synthesis, Functionalization, and Applications. *Acc. Chem. Res.* **2019**, *52*, 1598−1610.
(40) Tsotsalas, M.; Liu, J.; Tettmann, B.; Grosjean, S.; Shahnas, A.; Wang, Z.; Azucena, C.; Addicoat, M.; Heine, T.; Lahann, J.; Overhage, J.; Bräse, S.; Gliemann, H.; Wöll, C. Fabrication of Highly Uniform Gel Coatings by the Conversion of Surface-Anchored Metal−Organic Frameworks. *J. Am. Chem. Soc.* **2014**, *136*, 8−11.
(41) Wang, Z.; Błaszczyk, A.; Fuhr, O.; Heissler, S.; Wöll, C.; Mayor, M. Molecular weaving via surface-templated epitaxy of crystalline coordination networks. *Nat. Commun.* **2017**, *8*, 14442−14442.
(42) Hassan, Z.; Matt, Y.; Begum, S.; Tsotsalas, M.; Bräse, S. Assembly of Molecular Building Blocks into Integrated Complex Functional Molecular Systems: Structuring Matter Made to Order. *Adv. Funct. Mater.* **2020**, *30*, 1907625.
(43) Grosjean, S.; Hassan, Z.; Wöll, C.; Bräse, S. Diverse Multi-Functionalized Oligoarenes and Heteroarenes for Porous Crystalline Materials. *Eur. J. Org. Chem.* **2019**, *2019*, 1446−1460.
(44) Yang, Q.; Xu, Q.; Jiang, H.-L. Metal−organic frameworks meet metal nanoparticles: synergistic effect for enhanced catalysis. *Chem. Soc. Rev.* **2017**, *46*, 4774−4808.
(45) Yi, B.; Zhao, H.; Zhang, Y.; Si, X.; Zhang, G.; An, Y.; Su, L.; Tsung, C.-K.; Chou, L.-Y.; Xie, J. A direct solvent-free conversion approach to prepare mixed-metal metal−organic frameworks from doped metal oxides. *Chem. Commun.* **2021**, *57*, 3587−3590.
(46) Chui, S. S.-Y.; Lo, S. M.-F.; Charmant, J. P. H.; Orpen, A. G.; Williams, I. D. A Chemically Functionalizable Nanoporous Material $[Cu_3(TMA)_2(H_2O)_3]_n$. *Science* **1999**, *283*, 1148−1150.
(47) Kresse, G.; Furthmüller, J. Efficient iterative schemes for ab initio total-energy calculations using a plane-wave basis set. *Phys. Rev. B* **1996**, *54*, 11169−11186.
(48) Coupry, D. E.; Addicoat, M. A.; Heine, T. Extension of the Universal Force Field for Metal−Organic Frameworks. *J. Chem. Theory Comput.* **2016**, *12*, 5215−5225.
(49) Peralta, D.; Barthelet, K.; Pérez-Pellitero, J.; Chizallet, C.; Chaplais, G.; Simon-Masseron, A.; Pirngruber, G. D. Adsorption and Separation of Xylene Isomers: CPO-27-Ni vs HKUST-1 vs NaY. *J. Phys. Chem. C* **2012**, *116*, 21844−21855.
(50) Hassan, Z.; Spuling, E.; Knoll, D. M.; Lahann, J.; Bräse, S. Planar chiral [2.2]paracyclophanes: from synthetic curiosity to applications in asymmetric synthesis and materials. *Chem. Soc. Rev.* **2018**, *47*, 6947−6963.
(51) Hassan, Z.; Spuling, E.; Knoll, D. M.; Bräse, S. Regioselective Functionalization of [2.2]Paracyclophanes: Recent Synthetic Progress and Perspectives. *Angew. Chem., Int. Ed.* **2020**, *59*, 2156−2170.
(52) Hassan, Z.; Bräse, S. Metal-to-Metal Distance Modulation by Ligand Design: A Case Study of Structure-Property Correlation in Planar Chiral Cyclophanyl Metal Complexes. *Chem. − Eur. J.* **2021**, *27*, 15021−15027.
(53) Jackson, N.; Stam, F.; O'Brien, J.; Kailas, L.; Mathewson, A.; O'Murchu, C. Crystallinity and mechanical effects from annealing Parylene thin films. *Thin Solid Films* **2016**, *603*, 371−376.
(54) Mathur, M. S.; Weir, N. A. Laser raman and infrared spectrum of poly-p-xylylene. *J. Mol. Struct.* **1973**, *15*, 459−463.
(55) Dhumal, N. R.; Singh, M. P.; Anderson, J. A.; Kiefer, J.; Kim, H. J. Molecular Interactions of a Cu-Based Metal−Organic Framework with a Confined Imidazolium-Based Ionic Liquid: A Combined Density Functional Theory and Experimental Vibrational Spectroscopy Study. *J. Phys. Chem. C* **2016**, *120*, 3295−3304.
(56) Ferrari, A. C.; Robertson, J.; Castiglioni, C.; Tommasini, M.; Zerbi, G. Raman spectroscopy of polyconjugated molecules and materials: confinement effect in one and two dimensions. *Proc. R. Soc. London, Ser. A* **2004**, *362*, 2425−2459.
(57) Yan, Y.; Bein, T. Molecular sieve sensors for selective ethanol detection. *Chem. Mater.* **1992**, *4*, 975−977.
(58) Klimeš, J.; Bowler, D. R.; Michaelides, A. Van der Waals density functionals applied to solids. *Phys. Rev. B* **2011**, *83*, 195131.
(59) Verploegh, R. J.; Nair, S.; Sholl, D. S. Temperature and Loading-Dependent Diffusion of Light Hydrocarbons in ZIF-8 as Predicted Through Fully Flexible Molecular Simulations. *J. Am. Chem. Soc.* **2015**, *137*, 15760−15771.

(60) Pramudya, Y.; Bonakala, S.; Antypov, D.; Bhatt, P. M.; Shkurenko, A.; Eddaoudi, M.; Rosseinsky, M. J.; Dyer, M. S. High-throughput screening of metal−organic frameworks for kinetic separation of propane and propene. *Phys. Chem. Chem. Phys.* **2020**, *22*, 23073−23082.
(61) Henkelman, G.; Uberuaga, B. P.; Jónsson, H. A climbing image nudged elastic band method for finding saddle points and minimum energy paths. *J. Phys. Chem. C* **2000**, *113*, 9901−9904.
(62) Henkelman, G.; Jónsson, H. Improved tangent estimate in the nudged elastic band method for finding minimum energy paths and saddle points. *J. Phys. Chem. C* **2000**, *113*, 9978−9985.
(63) Kumar, S.; Pramudya, Y.; Müller, K.; Chandresh, A.; Dehm, S.; Heidrich, S.; Fediai, A.; Parmar, D.; Perera, D.; Rommel, M.; Heinke, L.; Wenzel, W.; Wöll, C.; Krupke, R. Sensing Molecules with Metal−Organic Framework Functionalized Graphene Transistors. *Adv. Mater.* **2021**, *33*, 2103316.
(64) Canepa, P.; Nijem, N.; Chabal, Y. J.; Thonhauser, T. Diffusion of Small Molecules in Metal Organic Framework Materials. *Phys. Rev. Lett.* **2013**, *110*, No. 026102.
(65) Senkevich, J. J.; Wiegand, C. J.; Yang, G.-R.; Lu, T.-M. Selective Deposition of Ultrathin Poly(p-xylene) Films on Dielectrics Versus Copper Surfaces. *Chem. Vap. Deposition* **2004**, *10*, 247−249.
(66) Vaeth, K. M.; Jensen, K. F. Transition Metals for Selective Chemical Vapor Deposition of Parylene-Based Polymers. *Chem. Mater.* **2000**, *12*, 1305−1313.
(67) Chen, H.-Y.; Lai, J. H.; Jiang, X.; Lahann, J. Substrate-Selective Chemical Vapor Deposition of Reactive Polymer Coatings. *Adv. Mater.* **2008**, *20*, 3474−3480.
(68) Nandivada, H.; Chen, H.-Y.; Lahann, J. Vapor-Based Synthesis of Poly[(4-formyl-p-xylylene)-co-(p-xylylene)] and Its Use for Biomimetic Surface Modifications. *Macromol. Rapid Commun.* **2005**, *26*, 1794−1799.
(69) Chen, H.-Y.; Lahann, J. Vapor-Assisted Micropatterning in Replica Structures: A Solventless Approach towards Topologically and Chemically Designable Surfaces. *Adv. Mater.* **2007**, *19*, 3801−3808.
(70) Jiang, X.; Chen, H.-Y.; Galvan, G.; Yoshida, M.; Lahann, J. Vapor-Based Initiator Coatings for Atom Transfer Radical Polymerization. *Adv. Funct. Mater.* **2008**, *18*, 27−35.
(71) Xie, F.; Deng, X.; Kratzer, D.; Cheng, K. C. K.; Friedmann, C.; Qi, S.; Solorio, L.; Lahann, J. Backbone-Degradable Polymers Prepared by Chemical Vapor Deposition. *Angew. Chem., Int. Ed.* **2017**, *56*, 203−207.
(72) Koenig, M.; Lahann, J. Vapor-based polymers: from films to nanostructures. *Beilstein J. Nanotechnol.* **2017**, *8*, 2219−2220.
(73) Hassan, Z.; Varadharajan, D.; Zippel, C.; Begum, S.; Lahann, J.; Bräse, S. Design Strategies for Structurally Controlled Polymer Surfaces via Cyclophane-Based CVD Polymerization and Post-CVD Fabrication. *Adv. Mater.* **2022**, DOI: 10.1002/adma.202201761.